Endurance Time Method for Rapid Collapse Safety Assessment of Earthquake-Damaged Buildings

Mohsen Kalateh-Ahani[a,*] and Homayoon E. Estekanchi[b]

[a.] *Department of Civil Engineering and Architecture, University of Torbat Heydarieh, Torbat Heydarieh, Iran.*
[b.] *School of Civil Engineering, Sharif University of Technology, Tehran, Iran.*

Abstract.

Post-earthquake building safety assessment must rapidly evaluate structural integrity before imminent aftershocks to guide safe reoccupation decisions. While studies have quantified residual collapse capacity following seismic damage, computational demands of conventional Incremental Dynamic Analysis (IDA) methods pose challenges for urgent, real evaluations. This research proposes an efficient framework using the Endurance Time (ET) method to estimate rapidly the residual collapse capacities needed for post-earthquake building safety assessment. The ET method leverages an incrementally scaled acceleration function in a single Nonlinear Response History Analysis (NRHA) to simulate the demands across intensity levels up to complete collapse. We develop a procedure adapting ET for mainshock-aftershock damage assessment, introducing Representative Damage States (RDSs) as an alternative to IDA's iterative analyses at fixed damage states. This paper demonstrates the framework's steps on a steel moment frame benchmark modeled with OpenSees and subjected to earthquake scenarios emulating the 2015 Nepal event. The findings show the ET method can efficiently generate the complete residual collapse capacity diagram for a mainshock-damaged building, covering all potential damage states with minimal nonlinear analyses. This computational efficiency is advantageous for overcoming barriers in emergency assessments, enabling rapid evaluation of building collapse safety after significant seismic events.

Keywords: endurance time method; incremental dynamic analysis; residual collapse capacity; mainshock-aftershock sequences; post-earthquake structural safety.

1. Introduction

Post-mainshock structural safety evaluations focus on whether a mainshock has damaged a building's integrity to the point where the remaining collapse capacity is insufficient to withstand strong aftershocks. If this is the case, the building is considered less safe than before the incident, and occupancy restrictions may be necessary [1-4]. Seismic codes generally simulate earthquake loading effects as a single event, allowing structures to experience limited damage, and neglecting the secondary damage that may be induced by aftershocks [3]. However, as noticeable in many earthquake disasters, the intervals between the mainshock and powerful aftershocks are sometimes not long enough to make repairs or retrofit of damaged structures possible [5]. For instance, in the 2015 Nepal earthquake, a strong aftershock with a magnitude M_w6.7 occurred just 58 minutes after the M_w7.8 mainshock. The strongest aftershock with a magnitude M_w7.3 was recorded 17 days later [6]. Developing efficient procedures for identifying structurally unsafe buildings immediately after a severe earthquake is crucial for emergency response efforts and can help reduce post-earthquake casualties.

* *Corresponding author.*
E-mail addresses: m.kalatehahani@torbath.ac.ir (*M. Kalateh-Ahani*), *stkanchi@sharif.edu* (*H.E. Estekanchi*).
Tel.: +985151240000(*168*), *+989388952244* (*M. Kalateh-Ahani*).

ATC-20 [7] evaluates the safety status of earthquake-damaged buildings and assigns green, yellow, and red tags via a visual damage inspection procedure. According to FEMA P-58 [8], if a building receives an unsafe placard, it has been damaged to the degree that entry, use, or occupancy poses a serious safety risk. In both the ATC-20 [7] and FEMA P-58 [8] methodologies, building inspectors conduct comprehensive visual inspections to estimate the level of damage to both structural and nonstructural components. Over the past 20 years, many studies have aimed to develop methods for quantifying the remaining collapse capacity of earthquake-damaged buildings. For instance, Bazzurro *et al.* [9] applied the pushover analysis method to generate collapse capacity curves for mainshock-damaged structures, while Luco *et al.* [10] compared the pushover analysis results with those from the back-to-back dynamic analysis and concluded that the dynamic approach yields more accurate estimates of collapse capacities than the static approach. The back-to-back dynamic analysis involves two Incremental Dynamic Analyses (IDAs): in the first IDA, the intensity of the mainshock excitation is gradually increased until the intact structure reaches a predetermined damage state, and in the second IDA, the intensity of the aftershock excitation is similarly increased until the mainshock-damaged structure collapses.

Several studies have been conducted to develop indices for estimating the residual collapse capacity of earthquake-damaged buildings and identifying the most effective engineering demand parameters for capturing additional damage induced by aftershocks. Ruiz-García and Aguilar [11] proposed an index based on residual inter-story drift ratios to estimate the residual collapse capacity of a four-story steel moment-frame building at five levels of post-mainshock damage states. Wen *et al.* [12] examined different engineering demand parameters for an earthquake-damaged five-story reinforced concrete frame building. They found that deformation-based demands were less sensitive to aftershocks, as the aftershocks' magnitudes are typically smaller than the mainshock. Tesfamariam and Goda [13] investigated a fifteen-story reinforced concrete frame building under earthquake sequences. They showed that hysteretic energy dissipation more accurately monitored the damage inflicted by aftershocks. Hysteretic energy dissipation is a cumulative damage indicator associated with cyclic-inelastic deformations in the seismic response of structures after yield occurs [14]. These studies [12, 13] confirmed that the Park-Ang damage index [15] outperforms other demand parameters in predicting the amount of damage accumulated during sequential earthquakes. The Park-Ang damage index combines the hysteretic energy dissipation demand with the deformation demand due to excessive lateral displacements [16]. Several recent studies have examined the Park-Ang damage index as a convenient seismic measure for various models of reinforced concrete and steel moment frame structures [3, 17-19].

Fewer studies have focused on developing methods for assessing whether the residual collapse capacity of an earthquake-damaged building is safe enough for reoccupation following a mainshock event. Raghunandan *et al.* [1] evaluated the collapse risk of four reinforced concrete frame buildings to quantify their post-mainshock vulnerability. They concluded that a building's collapse capacity is unaffected by aftershocks if it is not severely damaged in the mainshock. Still, collapse capacity is significantly reduced if it is extensively damaged. Zhang *et al.* [2] conducted the post-mainshock structural safety assessment of a four-story reinforced concrete frame building using a machine learning framework. They demonstrated that exploring the trend between the residual collapse capacity and peak inter-story drift ratio at different levels of post-mainshock damage states helps to specify the minimum threshold required to ensure collapse safety. Kalateh-Ahani and Amiri [4] investigated the application of the Park-Ang damage index in the collapse capacity analysis of a benchmark four-story steel moment-frame building. They generated IDA collapse capacity curves of the test building under a set of mainshock-aftershock sequences and incorporated them into a residual collapse capacity diagram.

Methods for evaluating the residual collapse capacity of earthquake-damaged buildings require significant computational efforts. These methods are typically based on IDAs requiring numerous Nonlinear Response History Analyses (NRHAs) under earthquake excitations incrementally scaled from a relatively lower intensity level to a level causing complete collapse. IDAs are usually performed for a group of selected earthquake sequences contributing to the site's seismic hazard potential to reduce the uncertainties inherent in dynamic analyses [4]. In the absence of such studies before the incident, the high computational demand of IDAs makes the collapse safety assessment of mainshock-damaged structures too time-consuming for real-world applications since strong aftershocks may occur within hours after the mainshock.

The Endurance Time (ET) method [20] provides an alternative for rapidly predicting seismic demands. This incremental-based dynamic time-history analysis involves subjecting structures to predesigned intensifying acceleration functions [21]. The ET method predicts structural responses in terms of the relationship between engineering demand parameters and the intensity of earthquakes at different levels. Unlike conventional NRHAs, which only provide computational outputs for a particular level, the ET method triggers structural responses to a continuous range of intensity levels using a single NRHA. The computational efficiency of the ET method has been successfully applied to the seismic response predictions of various structures in different areas of earthquake engineering [22-33].

The ET methodology uses simulated ground motion records for seismic predictions. Simulation of ground motion time histories has been extensively studied and applied for various purposes in seismic exploration. Rezaeian and Der Kiureghian [34] proposed a stochastic model based on a modulated filtered white-noise process to generate synthetic ground motions

matching specified earthquake and site characteristics. Rezaeian *et al.* [35] demonstrated applying a physics-based and stochastic simulation approach to model ground motions in the central and eastern United States over a wide range of magnitudes. Bradley *et al.* [36] guided verifying, validating, and documenting the utilization of simulated ground motions for engineering practice. Karimzadeh *et al.* [37] compared real and simulated ground motion records using alternative intensity measures, highlighting the significance of region-specific simulations. More recently, Arslan Kelam *et al.* [38] evaluated seismic hazard and potential damage for an urban area using site-specific models incorporating simulated ground motions consistent with regional source, velocity, and building characteristics.

Farivarrad and Estekanchi [27] recently applied the ET method for the seismic performance assessment of three reference steel moment-frame buildings of three, nine, and twenty stories subjected to mainshock-aftershock sequences. Although the ET method significantly reduces the computational time required for NRHAs, they observed that the accuracy of the ET method for predicting demand parameters under aftershocks reduces as the first-mode period of structures becomes longer. They reported that the ET method could acceptably predict the post-mainshock structural response of steel moment-frame buildings shorter than 35 meters.

Although studies have explored the residual collapse capacity of earthquake-damaged buildings for safe reoccupation after a mainshock event, to the best of our knowledge, no previous attempt has focused on developing rapid assessment methods to evaluate post-mainshock collapse safety to guide time-critical occupancy decisions. This research aims to address this gap by proposing a framework using the computationally efficient ET analysis method rather than IDA to estimate residual collapse capacity. We demonstrate the application of the ET method for rapid post-mainshock damage evaluation, leveraging the ability of ET analysis to efficiently predict seismic response across intensity levels, as validated through prior studies. This study demonstrates the steps of the proposed framework by modeling the collapse capacity analysis of a reference four-story steel moment-frame building. Additionally, the post-mainshock structural safety of the test building will be investigated following earthquake loading scenarios that replicate conditions during the 2015 Nepal earthquake event.

The remainder of this paper is organized as follows. Section 2 provides a brief overview of the fundamentals of the ET method. Section 3 shows how to evaluate the residual collapse capacity of mainshock-damaged structures. The procedure to assess post-mainshock collapse safety is then explained in Section 4. Section 5 summarizes the specifics of the steel moment frame modeled as a case study. Section 6 identifies representative damage states that will correlate the ET method with conventional back-to-back dynamic analyses. Results from implementing the proposed framework to estimate collapse capacities and structural safety evaluations under designated earthquake loading scenarios are presented and discussed in Section 7. Finally, Section 8 summarizes this study's key conclusions and contributions, along with recommendations for future work to extend applications of the proposed framework.

2. Endurance Time method

The cardiac exercise stress test inspired the Endurance Time (ET) method concept. This test monitors heart rate and blood pressure during incremental treadmill or cycle ergometer exercise until maximum intensities [21]. Similarly, the ET method subjects a structure to gradually increasing dynamic excitation until collapse. Seismic performance is assessed based on the structural response at each intensity level [21]. Figure 1 illustrates the ET technique. The successful implementation of the ET method relies on generating accurate Endurance Time Excitation Functions (ETEFs) that can simulate the effects of real ground motions from low to high intensity on the structural response. One straightforward approach to generating ETEFs is to find excitation functions that ensure the response spectrum corresponding to each time step matches the product of a target response spectrum and an intensifying function that represents different intensity levels, as expressed by:

$$S_a(t,T) = \frac{t}{t_{\text{target}}} S_a^{\text{target}}(T) \tag{1}$$

In Eq. (1), T is the first-mode period of vibration, $S_a(t,T)$ is the spectral acceleration of the excitation function from zero to a particular time t, and t_{target} is the target time to match a target spectrum, denoted as $S_a^{\text{target}}(T)$. The target spectrum can be either a code design spectrum or a mean spectrum of a set of ground motions. For example, the ETEF model in Fig. 1 has a target time of 10 seconds, so the spectral acceleration of the 0-10 second ETEF corresponds to a target spectrum for the seismic hazard level of a 10% probability of exceedance in 50 years.

Generating ETEFs satisfying Eq. (1) requires robust optimization due to highly constrained, multimodal search spaces with numerous local optima. Various metaheuristic algorithms have successfully addressed this over the past decade, developing five ETEF generations with different target spectra for earthquake engineering needs like performance-based design/retrofit, lifecycle cost design, reliability, and safety assessment [39-41]. Studies show current ETEFs reasonably estimate structural responses at different seismic intensities with minimal computation [22-33]. A review of the five ETEF generations and detailed specifications is available in [21].

This study uses the fifth "ETA20kd" ETEF generation [41] to form mainshock-aftershock sequences for nonlinear response history analysis (NRHA). It includes three records: "ETA20kd01", "ETA20kd02", and "ETA20kd03". The ET simulation process of this generation used the average response spectrum of the far-field record set (consisting of 22 pairs of ground motion records) of FEMA P695 [42] as the target response spectrum. These ground motions were selected from events greater than M_w6.5 at sites with different types of soils located at a distance greater than 10 kilometers from fault rupture. Mashayekhi *et al.* [41] compared the ETA20kd damage spectra to FEMA-695's far-field set using the Park-Ang damage index, demonstrating good compatibility. They reported 96% accuracy in predicting incremental dynamic analysis results, with less than 1% of the computational time.

3. Collapse capacity analysis of earthquake-damaged buildings

To evaluate residual collapse capacity after mainshock damage, represented by the kappa index, the aftershock intensity causing collapse is normalized to the collapse intensity of the intact structure [4]. Two methods determine this: 1) using the mainshock to find the intact structure's collapse capacity [11], or 2) using the aftershock [2]. Method 1 yields kappa values <1 or >1, while Method 2 scales kappa between 0 and 1 [4]. This study adopts Method 2, providing a fixed 0-1 scale for kappa, representing the same remaining aftershock capacity, regardless of the mainshock input.

Most previous studies on collapse capacity analysis of structures damaged by mainshocks have used the spectral acceleration at the first-mode period $Sa(T_1)$ as the seismic intensity measure. However, in this study, we employ the spectral acceleration averaged over a range of periods Sa_{ave}. In a survey by Eads *et al.* [38], nearly 700 moment-frame and shear wall buildings of various heights were examined to compare the effectiveness and sufficiency of these two alternatives, $Sa(T_1)$ and Sa_{ave}. The authors reported that the measure Sa_{ave} is approximately 40% more efficient in predicting the structural response and yields relatively stable estimates of collapse risk, even with different ground motion sets, reflecting its sufficiency. This parameter is computed as the geometric mean of spectral acceleration values between periods c_1T_1 and c_nT_1, as follows [43]:

$$Sa_{ave}(c_1T_1,\ldots,c_nT_1)=\left(\prod_{i=1}^{n}Sa\left(c_iT_1\right)\right)^{1/n} \tag{2}$$

In Eq. (2), the terms c_i represent non-negative values, and *n* is the total number of these values. This study considers the 5%-damped response spectral values and computes the parameter Sa_{ave} using a period range between $0.2T_1$ and $3.0T_1$ seconds, with a uniform period spacing of 0.01 seconds. This specific period range was chosen based on Eads *et al.* [43], who reported it generally yielded good results for the efficiency and sufficiency of Sa_{ave} as an intensity measure concerning collapse prediction.

The residual collapse capacity of a structure damaged by a mainshock to withstand an aftershock can be quantified by the kappa index as:

$$\kappa=\frac{Sa^{AS}_{ave,\,DMG}}{Sa^{AS}_{ave,\,INT}} \tag{3}$$

where $Sa^{AS}_{ave,\,DMG}$ and $Sa^{AS}_{ave,\,INT}$ denote the intensities of the averaged spectral acceleration that correspond to the collapse

capacity of the damaged and intact structures, respectively, under the excitation of the aftershock. These two intensities are obtained by two separate IDAs required to test different intensity levels of the excitation record, each level through a separate NRHA, as demonstrated in [2, 4, 11, 44]. However, using the ET method, each collapse capacity can be identified through a single NRHA, as each ETEF provides structural responses to the entire range of intensity up to the collapse level. This study uses the Park-Ang damage index to measure the damage experienced by the case-study building under ETEFs. The details of the Park-Ang damage index calculations and the interpretation of different levels of damage are reviewed in [4].

4. Assessing structural safety with residual collapse capacity index

An alternative approach assesses earthquake-damaged buildings' residual collapse capacity [2-4,45]. The kappa index variation with increasing mainshock damage intensity is visualized. Residual capacities are calculated at predefined damage states, with other kappa values linearly interpolated. Curves are generated for selected mainshock-aftershock sequences contributing to site seismic hazard, then averaged into one curve. This estimates the kappa index based on measured mainshock damage intensity. Post-mainshock safety classification compares the estimated kappa to a minimum threshold $\kappa_{\min}$, checking if residual capacity allows safe re-occupancy [4].

As mentioned in Section 2, for the case-study building, the set of mainshock-aftershock sequences needed to generate the residual collapse capacity diagram is created using the hysteretic-energy-compatible ETEFs, specifically the "ETA20kd" series. This set consists of 12 earthquake sequences with specific IDs, as listed in Table 1. Each sequence contains one of the three "ETA20kd" excitation records as the mainshock and the other two, with positive or negative polarity as the aftershock. The polarity of the aftershock is investigated in this study since several works, such as [1, 11, 46], have reported that negative polarity can significantly affect residual drift or displacement. A similar effect will likely occur when the Park-Ang damage index is accounted for as the seismic demand.

Experimental studies are needed to reliably determine the minimum kappa threshold ensuring the collapse safety of earthquake-damaged buildings. According to Burton and Sharma [3], setting the mainshock damage safety threshold is a policy decision like FEMA P695 [42] adopting 10% collapse probability at the maximum considered earthquake. However, the lack of experimental evidence limits minimum kappa suggestions to numerical investigations. Raghunandan *et al.* [1] reported minor mainshock structural damage doesn't significantly affect the remaining aftershock capacity. Similarly, Zhang *et al.* [2] proposed damage severity is insignificant for continued occupancy until the residual capacity curve remains relatively flat. This study adopts the Park-Ang "minor damage" classification to determine a safety threshold distinguishing safe and unsafe states.

5. Case study: four-story steel office building

The case-study building is a four-story steel office assumed to be located in Los Angeles, USA, with a floor system consisting of a composite metal deck with a lightweight concrete slab. The building is a benchmark model developed by Lingnos [47] for analyzing the collapse capacity of steel moment-frame structures. Different perspectives of the building are illustrated in Figure 2. As shown in Figure 2(b), the seismic force-resisting systems of the building consist of two two-bay moment frames in the east-west direction and two three-bay moment frames in the north-south direction. In this study, we examine the special moment frame located at grid A(2-4), whose geometry, including dimensions and cross-sections of the beams and columns, is depicted in Figure 2(d). All beams and columns are rolled W-sections selected from ASTM A6 [48]. The moment frame connections are Reduced Beam Section (RBS) connections designed following FEMA-350 [49] criteria.

The A(2-4) moment frame computer model is created and analyzed in OpenSees [50]. A leaning column linked by rigid trusses simulates P-Delta effects from gravity loads on adjacent interior frames, as shown in Figure 2(d). Panel zones at beam-column intersections are modeled using "elemPanelZone2D". The model's first three periods are 0.8509s, 0.2817s, and 0.1361s. The modified Ibarra-Medina-Krawinkler (IMK) deterioration model [51] simulates beam-column connection nonlinear moment-rotation behavior. The composite steel beams with RBS have asymmetric moment-rotation due to the concrete slab. Elkady and Lignos [52] calibrated the IMK input parameters using experimental composite RBS beam

hysteresis. Their modification factors adapt the bare steel RBS IMK model for the slab contribution. Further OpenSees modeling and seismic considerations are provided in [4,47].

6. Adapting the ET method for mainshock-aftershock damage assessment

During a back-to-back dynamic analysis, the response history of a typical structure under a real mainshock excitation is generally expected to gradually converge to a steady-state value. This means the structural velocity eventually tends to zero as the ground acceleration begins to fade. Therefore, the structure enters the free-vibration phase with near-zero velocity, and its oscillation is quickly damped due to the inherent damping characteristic. As a result, the cumulative damage measured at the end of the mainshock excitation should remain constant during the free vibration of the structure.

As mentioned earlier, the basic idea of the ET analysis is to produce a range of structural responses from elastic to plastic and even collapse through a single NRHA. A specific intensifying dynamic function is used rather than repeatedly scaling an earthquake excitation for each intensity level and running multiple NRHAs as required for IDA procedures. Unlike a real earthquake excitation that fades to zero, an ET excitation function is progressively intensified. Thus, when an ETEF is used for back-to-back dynamic analysis, the structure may begin the free-vibration phase with considerable initial velocity, increasing the cumulative damage measured at the end of the mainshock excitation. Increasing the damage index during the free vibration phase leads to numerical inaccuracies in estimating the remaining capacity of mainshock-damaged structures to withstand aftershocks. This issue influences the numerical stability of the ET method for mainshock-aftershock damage assessment.

To address this issue, we propose using a set of varying and non-consecutive damage states, chosen through a step-by-step procedure, as an alternative to the fixed, consecutive damage states typically employed in IDA methods. This procedure selects damage intensities from the response history of a mainshock-damaged structure as representative damage states that meet two conditions: first, the response history remains steady for a predefined time after them; second, they are distributed as uniformly as possible. Since the imposed dynamic loading intensity increases with time in an ETEF, the first condition helps prevent potential problems during the free-vibration phase. Meanwhile, the second condition produces a more uniform selection of the damage states. The procedure is as follows:

1. Obtain the response history of the damage measure for the ETEF used as the mainshock excitation.
2. Identify all plateaus in the diagram with a duration longer than a predefined value cT_1.
3. Consider the damage intensity at the onset of each plateau as a candidate for the damage states.
4. Find the nearest candidates to a set of fixed-distance damage intensities between zero and the collapse level and sort them in ascending order.
5. Remove any candidate from the sequence closer to its predecessor than the fixed interval used in Step 4.
6. The remaining candidates are the Representative Damage States (RDSs).

As mentioned in Section 3, we use the Park-Ang damage index to measure the damage experienced by the test building, taking the damage states in Step 4 at intervals of [0, 0.77] with a fixed distance of 0.05. We find a practical value of 0.25 for the parameter *c* sufficient to select the required candidates in Step 2. The damage histories of the test building, subjected to the three excitation records of the "ETA20kd" series, and the damage states, represented by the proposed procedure, are illustrated in Figure 3. In this figure, the ordinate of the graph *DI* represents the measured Park-Ang damage index. The RDSs, as shown in Figure 3, differ in their magnitude and number for each excitation record. In the following section, we will use these specifically chosen damage states for the back-to-back dynamic analysis of the test building rather than using fixed damage states, as is typical in IDA methods.

7. Collapse capacity analysis of the case-study building: results and diagrams

7.1. Residual collapse capacity diagram

The seismic collapse capacity curve illustrates how a response parameter varies with the intensity level of an excitation record as it progressively increases until structural collapse occurs. Collapse capacity curves for the test building were generated by conducting back-to-back dynamic analyses using the twelve earthquake sequences detailed in Table 1. The intensity level is scaled using the averaged spectral acceleration Sa_{ave}, and the structural response is evaluated using the Park-Ang damage index. When using an ETEF as the excitation record instead of a real excitation, a single NRHA is sufficient to cover the entire range of intensity levels. This feature of the ET method saves considerable time and effort in predicting collapse capacities. According to the first author's prior experience with seismic simulation of the same test building, as documented in [4], producing a single IDA-based collapse capacity curve for the test building takes at least 24 times longer than using the ET method.

Figure 4 displays a series of collapse capacity plots for the intact and mainshock-damaged structures at different damage state levels. Each row in Figure 4 corresponds to one of the three excitation records from the "ETA20kd" series, used as the mainshock in the simulated earthquake sequence. Each row of this figure contains two diagrams, with the other two records of the "ETA20kd" series used as the aftershock, each shown with positive and negative polarity. Each curve in Figure 4 is generated by analyzing the intact structure under the mainshock excitation until its damage history reaches one of the RDSs defined in Figure 3. Once a predefined damage state is reached, after 20 sec of free vibration, the second NRHA is conducted by applying the aftershock excitation until the collapse point is reached. In the diagrams of Figure 4, the green curves represent a theoretical scenario where the intact structure suffered no damage under the mainshock, with only the aftershock used to generate the curve. The orange and blue curves represent the positive and negative polarities of the aftershock, respectively.

Figure 5 shows the collapse capacity of the mainshock-damaged structure for the positive and negative polarities of the aftershock at the RDSs used to generate the orange and blue curves in Figure 4. The relative change in collapse capacity between the positive and negative polarities is also reported in Figure 5 for each RDS. The green values indicate that the negative polarity resulted in a higher collapse capacity than the positive polarity, and vice versa for the red values. The average red values observed across all diagrams in Figure 5 suggest that without considering negative polarity, the collapse capacity of the earthquake-damaged building may be overestimated. However, the relatively small average values reveal that the difference appears insignificant for the test building.

Figure 6(a) depicts the residual collapse capacity diagram of the test building exposed to the earthquake sequences in Table 1 for the worst-case polarity, *i.e.*, the polarity with a lower collapse capacity, at the selected RDSs for each ETEF. The diagram in Figure 6(b) displays the mean values of the kappa index, interpolated over a range of damage states between zero and the collapse level. Each curve in Figure 6(a) starts at 1, indicating the undamaged structure under the mainshock (*DI*=0), and decreases to 0, indicating the collapsed structure under the mainshock (*DI*=0.77). The residual collapse capacity reductions calculated at different damage states are illustrated in Figure 6(b) using red bars, with the percent reduction value reported at the top of each corresponding bar.

As mentioned in Section 4, obtaining a dependable value for the minimum residual collapse capacity threshold that ensures the structural safety of mainshock-damaged buildings requires extensive experimental validation studies. Without such comprehensive experimental data, the "minor damage level" of the Park-Ang damage index can provide a reasonable starting point to estimate the minimum threshold. Figure 7 shows that if the *DI* value of 0.11 (for details, refer to Table 1 of [4]) is set as the maximum acceptable damage index at which the test building can still be deemed safe for continued occupancy, the minimum kappa safety threshold is estimated to be 0.96. In other words, a maximum permissible reduction of 4% in the residual collapse capacity is allowable without compromising the structural integrity of the mainshock-damaged building in terms of collapse safety. This estimated 4% reduction limit arises from the specific conditions of the test building analyzed in this study. Further analytical and experimental research across more structural conditions would be valuable to validate the 0.96 minimum kappa safety threshold suggested here more rigorously based on the minor damage classification.

7.2. Scenario earthquakes

This section examines the damage response of the test building when subjected to hypothetical scenario earthquakes to demonstrate how the residual collapse capacity diagram can help evaluate structural safety after a seismic event. Let us consider the Nepal M_w7.8 mainshock (Date: 2015.04.25, Station: Kanti Path) occurring at the test building site. After 20 seconds of free vibration, the Nepal M_w7.3 aftershock (Date: 2015.05.12, Station: Kanti Path) strikes. According to FEMA-350 [49], two levels of seismic hazard ground motions, the Design Basis Earthquake (DBE) and the Maximum Considered Earthquake (MCE), are used to assess the seismic performance of steel moment-frame structures. These represent ground

motions with a 10% and 2% probability of exceedance in 50 years, respectively. The scale factors required to match the Nepal M_w7.8 mainshock excitation to the DBE and MCE hazard levels can be directly determined from FEMA-350 specifications. However, FEMA-350 does not provide explicit guidance on scaling the aftershock excitation to specific hazard levels.

Li and Ellingwood [53] studied 30 mainshock earthquake records representing the 10%/50 yr and 2%/50 yr seismic hazards in Los Angeles, USA. They reported that applying scale factors of 0.90 and 0.91 to the DBE- and MCE-scaled mainshock excitations reasonably simulated aftershock excitations at seismic hazard levels of 15% and 3% probability of exceedance in 50 years, respectively. This study investigates the Nepal mainshock-aftershock sequence at two scenarios with different seismic hazard levels: first, the 10%/50 yr level for the mainshock and the 15%/50 yr level for the aftershock; next, the 2%/50 yr level for the mainshock and the 3%/50 yr level for the aftershock. We implement Li and Ellingwood's [53] method for scaling the aftershock excitation, except using the real recorded aftershock rather than simulating it from the mainshock. To prepare aftershocks for the two scenario earthquakes, first, the Nepal M_w7.3 aftershock is scaled to 10%/50 yr and 2%/50 yr levels per FEMA-350, then scaled down by factors of 0.90 and 0.91 to the 15%/50 yr and 3%/50 yr levels, respectively.

Figure 8 illustrates the damage histories of the test building under the two earthquake scenarios. The Park-Ang damage index values recorded at the end of the mainshock and aftershock excitations, for both positive and negative aftershock polarities, are noted in Figure 8. Using the generated mean kappa index diagram for the test building, Figure 9 displays the estimated residual collapse capacities of the mainshock-damaged structure under the Nepal M_w7.8 mainshock scaled to the DBE and MCE hazard levels as 0.92 and 0.73, respectively. Both values fall below the minimum residual collapse capacity threshold $\kappa_{\min} = 0.96$, indicating insufficient remaining capacity to ensure continued occupational safety if the Nepal M_w7.8 mainshock occurs at either hazard level of 10%/50 yr and 2%/50 yr.

However, the collapse risk differs for the two scenarios. In the first scenario, as shown in Figure 8(a), the mainshock-damaged structure can withstand the 15%/50 yr Nepal M_w7.3 aftershock since the recorded damage index after the aftershock remains below the collapse level. In the second scenario, as seen in Figure 8(b), the 3%/50 yr Nepal M_w7.3 aftershock can cause structural collapse, as the damage index exceeds the collapse level. The damage levels align with the estimated residual capacities for the two scenarios. In the first scenario earthquake, the relatively minor 8% reduction in residual collapse capacity under the 10%/50 yr mainshock suggests the mainshock-damaged structure is much more likely to resist collapse under the 15%/50 yr aftershock. In the second scenario earthquake, the relatively major 27% reduction under the 2%/50 yr mainshock results in a lack of remaining capacity to prevent collapse under the 3%/50 yr aftershock.

8. Concluding remarks and recommendations

This paper develops a framework for rapid post-mainshock collapse safety assessment, which can help structural engineers assess the residual collapse capacity of earthquake-damaged buildings more efficiently than existing IDA-based frameworks. The proposed framework achieves computational efficiency by adopting the ET analysis method. Unlike IDA methods requiring numerous incremental NRHAs, the ET method needs only a minimal number of NRHAs to generate the residual collapse capacity diagram. The framework uses averaged spectral acceleration to measure seismic intensity and the Park-Ang damage index to quantify damage intensity. A case study implementing the framework on a benchmark four-story steel moment frame building under two simulated earthquake scenarios based on the 2015 Nepal events demonstrates its applicability in practical, real-world situations. The case study findings lead to the following conclusions and recommendations for future work:

- Using the ET method for back-to-back dynamic analysis requires special adaptations. With an ET excitation function treated as the mainshock, the cumulative damage measured at the end of the excitation may increase during free vibration, causing numerical inaccuracies in calculating the residual collapse capacity index. One practical solution is using a set of specifically chosen damage states, called Representative Damage States (RDSs), rather than the fixed, consecutive damage states typically used in IDA methods. We have presented a straightforward procedure to identify RDSs for applying the ET analysis to mainshock-aftershock damage assessment. The results show this procedure can determine a set of RDSs for each ETEF, resolving the free vibration issue and promoting the near-uniform distribution of damage states.
- We investigated the effect of aftershock polarity on damage assessment of the test building. Our results show that incorporating negative polarity is important for obtaining realistic collapse capacity estimates. However, the differences between positive and negative polarities are not statistically significant for the "ETA20kd" series-based earthquake sequences applied to the test building.
- To generate the residual collapse capacity curves of the test building subjected to the 12 earthquake sequences defined for

the case study, we performed a total of 82 nonlinear response history analyses. This number of NRHAs is far fewer than what conventional IDA-based frameworks typically require for the same number of earthquake sequences. For example, under the sequence ID kd0102+ for the post-mainshock damage state of RDS=0.128 (refer to Figure 4(a)), collapse occurs at an averaged spectral acceleration of 1.0*g*. If increments of 0.05*g* are used for scaling this earthquake sequence, the IDA method requires at least 20 NRHAs to reach the collapse point. In contrast, the ET method can provide the seismic demand across the full intensity range up to collapse through just a single NRHA.

- Our analysis of the two earthquake scenarios reveals the following: In the first scenario, the higher residual collapse capacity of 0.92 estimated for the test building under the 10%/50 Nepal M_w7.8 mainshock implies the probable adequate remaining capacity to resist strong aftershocks, since the damage index of 0.50 recorded under the subsequent 15%/50 yr Nepal M_w7.3 aftershock falls below the collapse level. However, in the second scenario, the lower residual collapse capacity of 0.73 under the 2%/50 Nepal M_w7.8 mainshock suggests the insufficient remaining capacity to withstand strong aftershocks, as evidenced by the damage index of 1.17 exceeding the collapse level when subjected to the 3%/50 yr Nepal M_w7.3 aftershock.
- The case study confirms that the ET method can reasonably estimate residual collapse capacities at the damage states the test building may experience under the Nepal M_w7.8 mainshock excitation scaled to 10%/50 yr and 2%/50 yr hazard levels. The findings demonstrate promise for addressing computational barriers in assessing the collapse safety of earthquake-damaged buildings. However, this work represents an initial investigation into utilizing the ET method as an efficient simulation tool for rapidly evaluating building reoccupation safety after significant earthquakes. Further research is recommended to validate the reliability of the proposed framework across various practical conditions, including testing multiple reinforced concrete or steel seismic force-resisting structural systems from low to high-rise buildings, examining diverse earthquake scenarios ranging from near- to far-fault events with varying energy and frequency characteristics, physical collapse validation through shake table experiments, and investigating different damage measures.
- This study utilizes the minor damage level of the Park-Ang damage index to estimate a minimum kappa safety threshold for classifying earthquake-damaged buildings as safe or unsafe for continued occupancy. However, rigorously determining residual collapse capacity reduction limits that maintain structural safety remains an open question. Addressing this question through comprehensive numerical and experimental studies focused on refining and validating the minimum kappa safety threshold is essential before applying the proposed framework to practical post-earthquake evaluation projects. While this study suggests a framework for rapid post-mainshock safety assessment, determining a reliable quantitative basis for relating measured damage states to minimum safe residual collapse capacities should be a priority of future research.

Acknowledgments

The authors gratefully acknowledge the financial support provided by the University of Torbat Heydarieh through Grant No. UTH:2022.03.12.143780. The first author wishes to thank Saeed Amiri for sharing invaluable insights and contributions that assisted the research.

References

1. Raghunandan, M., Liel, A.B. and Luco, N. “Aftershock Collapse Vulnerability Assessment of Reinforced Concrete Frame Structures”, *Earthquake Engineering and Structural Dynamics*, **44**(3), pp. 419-439 (2015). https://doi.org/10.1002/eqe.2478
2. Zhang, Y., Burton, H.V., Sun. H., et al. “A Machine Learning Framework for Assessing Post-Earthquake Structural Safety”, *Structural Safety*, **72**, pp. 1-16 (2018). DOI:10.1016/j.strusafe.2017.12.001
3. Burton, H.V. and, Sharma, M. “Quantifying the Reduction in Collapse Safety of Mainshock–damaged Reinforced Concrete Frames with Infills”, *Earthquake Spectra*, **33**(1), pp. 25-44 (2017). DOI:10.1193/121015EQS179M
4. Kalateh-Ahani, M. and Amiri, S. “A Park-Ang Damage Index-based Framework for Post-mainshock Structural Safety Assessment”, *Structures*, **33**, pp. 820–829 (2021). http DOI:10.1016/j.istruc.2021.04.039
5. Ding, H., Zhou, Y., Ge, Z., et al. “High-resolution seismicity imaging and early aftershock migration of the 2023 Kahramanmaraş (SE Türkiye) MW7.9 & 7.8 earthquake doublet”, *Earthquake Science*, **36**(6), pp. 417-432 (2023). DOI:10.1016/j.eqs.2023.06.002
6. CESMD, “Center for Engineering Strong Motion Database”, US Geological Survey. https://strongmotioncenter.org
7. ATC-20, “Post-earthquake Building Safety Evaluation Procedures”, Applied Technology Council, Redwood City, USA, (1995).
8. FEMA P-58, “Seismic Performance Assessment of Buildings”, Federal Emergency Management Agency, Washington, DC, USA, (2012).
9. Bazzurro, P., Cornell, C.A., Menun, C., et al. “Guidelines for Seismic Assessment of Damaged Buildings”, *13th World Conference on Earthquake Engineering*, Vancouver, Canada, (2004).

10. Luco, N., Gerstenberger, M.C., Uma, S.R., et al. "A Methodology for Post-mainshock Probabilistic Assessment of Building Collapse Risk", *9th Pacific Conference on Earthquake Engineering*, Auckland, New Zealand (2011).
11. Ruiz- García, J. and Aguilar, J.D. "Aftershock Seismic Assessment Taking into Account Post-mainshock Residual Drifts", *Earthquake Engineering and Structural Dynamics*, **44**(9), pp. 1391-1407 (2014). DOI:10.1002/eqe.2523
12. Wen, W., Zhai, C., Ji, D., et al. "Framework for the Vulnerability Assessment of Structure Under Mainshock-Aftershock Sequences", *Soil Dynamics and Earthquake Engineering*, **101**, pp. 41-52 (2017). DOI:10.1016/j.soildyn.2017.07.002
13. Tesfamariam, S. and Goda, K. "Energy-Based Seismic Risk Evaluation of Tall Reinforced Concrete Building in Vancouver, BC, Canada, under M9 Megathrust Subduction Earthquakes and Aftershocks", *Frontiers in Built Environment*, **3**, pp. 1-17 (2017). DOI:10.3389/fbuil.2017.00029
14. Kaveh, A., Kalateh-Ahani, M. and Fahimi-Farzam, M. "Damage-based Optimization of Large-scale Steel Structures", *Earthquake and Structures*, **7**(9), pp. 1119-1139 (2014). DOI:10.12989/eas.2014.7.6.1119
15. Park, Y.J. and Ang, A.H. "Mechanistic Seismic Model for Reinforced Concrete", *Journal of Structural Engineering*, **111**(4), pp. 722-739 (1985). DOI:10.1061/(ASCE)0733-9445(1985)111:4(722)
16. Kaveh, A., Fahimi-Farzam, M. and Kalateh-Ahani, M. "Optimum design of steel frame structures considering construction cost and seismic damage", *Smart Structures and Systems*, **16**(1), pp. 1-26 (2015). DOI:10.12989/sss.2015.16.1.001
17. Lakhade, S. O., Kumar, R. and Jaiswal, O.R. "Estimation of drift limits for different seismic damage states of RC frame staging in elevated water tanks using Park and Ang damage index", *Earthquake Engineering and Engineering Vibration*, **19**(1), pp. 161-177 (2020). DOI:10.1007/s11803-020-0554-1
18. Alibabaei Shahraki, M., Kamgar, R. and Heidarzadeh, H. "Damage-based design of multiple tuned mass dampers to improve the seismic performance of steel frame structures", *Soil Dynamics and Earthquake Engineering*, **173**, pp. 108062 (2023). DOI:10.1016/j.soildyn.2023.108062
19. Alibabaei Shahraki, M., Kamgar, R. and Heidarzadeh, H. "Assessing the seismic behavior of structures controlled with a novel elastoplastic-tuned mass damper inerter considering the effects of soil-structure interactions", *Structures*, **57**, pp. 105265 (2023). DOI:10.1016/j.istruc.2023.105265
20. Estekanchi, H.E., Vafai, H.A. and Sadeghazar, M. "Endurance Time Method for Seismic Analysis and Design of Structures", *Scientia Iranica*, **11**(4), pp. 361–370 (2004).
21. Estekanchi, H.E., Mashayekhi, M., Vafai, H.A., et al. "A State-of-knowledge Review on the Endurance Time Method", *Structures*, **27**, pp. 2288-2299 (2020). DOI:10.1016/j.istruc.2020.07.062.
22. Estekanchi, H.E., Arjomandi, K., Vafai, H.A. "Estimating structural damage of steel moment frames by endurance time method", *Journal of Constructional Steel Research* 2008;64(2):145–155. DOI:10.1016/j.jcsr.2007.05.010
23. Basim, MC and Estekanchi, H.E. "Application of Endurance Time Method in Performance-based Optimum Design of Structures", *Structural Safety*, **56**, pp. 52–67 (2015). DOI:10.1016/j.strusafe.2015.05.005
24. Rahimim, E. and Estekanchi, H.E. "Collapse Assessment of Steel Moment Frames Using Endurance Time Method", *Earthquake Engineering and Engineering Vibration*, **14**(2), pp. 347-360 (2015). DOI:10.1007/s11803-015-0027-0
25. Estekanchi, H.E., Vafai, H.A. and Basim, MC "Design and assessment of seismic resilient structures by the endurance time method", *Scientia Iranica*, **23**(4), pp. 1648-1657 (2016). DOI:10.24200/SCI.2016.2236
26. Estekanchi, H.E., Harati, M. and Mashayekhi, M.R. "An investigation on the interaction of moment-resisting frames and shear walls in RC dual systems using endurance time method", *The Structural Design of Tall and Special Buildings*, **27**(12), pp. e1489 (2018). DOI:10.1002/tal.1489
27. Farivarrad, A.H. and Estekanchi, H.E. "Seismic Performance Assessment of SMRF Structures Subjected to Mainshock-Aftershock Seismic Sequences by Endurance Time Method", *Journal of Earthquake Engineering*, **26**(7), pp. 3281-3299 (2020). DOI:10.1080/13632469.2020.1798828.
28. Pang, Y. and Wang, X. "Enhanced Endurance-time-method (EETM) for Efficient Seismic Fragility, Risk and Resilience Assessment of Structures", *Soil Dynamics and Earthquake Engingeering*, **147**, pp. 106731 (2021). DOI:10.1016/j.soildyn.2021.106731.
29. Mashayekhi, M.R., Estekanchi, H.E. and Vafai, H.A. "Optimal objective function for simulating endurance time excitations", *Scientia Iranica*, **27**(4), pp. 1728-1739 (2020). DOI:10.24200/SCI.2018.5388.1244
30. Davari, S. and Estekanchi, H.E. "Estimating the response of concrete moment frames subjected to individual ground motions using endurance time excitation functions fitted to average acceleration response spectra", *Scientia Iranica*, **28**(6), pp. 3008-3017 (2021). DOI:10.24200/SCI.2021.55649.4331
31. Estekanchi, H.E. and Vafai, H.A. "Seismic Analysis and Design using the Endurance Time Method", Ed. 2nd, Taylor & Francis Group, CRC Press, Folrida, USA (2021).
32. Estekanchi, H.E., Mashayakhi, M.R. and Vafai, H.A. "Endurance Time Excitation Functions: Intensifying Dynamic Loads for Seismic Analysis and Design", Ed. 1st, Taylor & Francis Group, CRC Press, Folrida, USA (2022).
33. Ashrafifar, A. and Estekanchi, H.E. "Life-cycle seismic fragility and resilience assessment of aging bridges using the endurance time method", *Soil Dynamics and Earthquake Engineering*, **164**, pp. 107524 (2023). DOI:10.1016/j.soildyn.2022.107524.
34. Rezaeian, S. and Der Kiureghian, A. "Simulation of synthetic ground motions for specified earthquake and site characteristics", *Earthquake Engineering and Structural Dynamics*, **39**(10), pp. 1155-1180 (2010). DOI:10.1002/eqe.997
35. Rezaeian, S., Hartzell, S., Sun, X., et al. "Simulation of Earthquake Ground Motions in the Eastern United States Using Deterministic Physics- Based and Site- Based Stochastic Approaches", *Bulletin of the Seismological Society of America*, **107**(1), pp. 149-168 (2016). DOI:10.1785/0120160031
36. Bradley, B.A., Pettinga, D., Baker, J.W., et al. "Guidance on the Utilization of Earthquake-Induced Ground Motion Simulations in Engineering Practice", *Earthquake Spectra*, **33**(3), pp. 809-835 (2017). DOI:10.1193/120216eqs219ep

37. Karimzadeh, S., Kadas, K., Askan, A., and et al. “Comparison of real and simulated records using ground motion intensity measures”, *Soil Dynamics and Earthquake Engineering*, **147**, pp. 106796 (2021). DOI:10.1016/j.soildyn.2021.106796
38. Arslan Kelam, A., Karimzadeh, S., Yousefibavil, K., et al. “An evaluation of seismic hazard and potential damage in Gaziantep, Turkey using site specific models for sources, velocity structure and building stock”, *Soil Dynamics and Earthquake Engineering*, **154**, pp. 107129 (2022). DOI:10.1016/j.soildyn.2021.107129
39. Kaveh, A., Kalateh-Ahani, M. and Estekanchi, H.E. “Production of Endurance Time Excitation Functions: the CMA Evolution Strategy Approach”, *Iranian Journal of Science and Technology, Transactions of Civil Engineering*, **37**(C+), pp. 383-94 (2013). DOI:10.22099/IJSTC.2013.1794
40. Mashayekhi, M., Estekanchi, H.E., Vafai, H.A., et al. “An Evolutionary Optimization-based Approach for Simulation of Endurance Time Load Functions”, *Optimization and Engineering*, **51**(12), pp. 2069-2088 (2019). DOI:10.1080/0305215X.2019.1567724
41. Mashayekhi, M., Estekanchi, H.E., Vafai, H.A., et al. “Development of Hysteretic Energy Compatible Endurance Time Excitations and Its Application”, *Engineering Structures*, **177**, pp. 753-769 (2018). DOI:10.1016/j.engstruct.2018.09.089
42. FEMA P695, “Quantification of Building Seismic Performance Factors”, Federal Emergency Management Agency, Washington, DC, USA, (2009).
43. Eads, L., Miranda, E. and Lignos, D.G. “Average Spectral Acceleration as an Intensity Measure for Collapse Risk Assessment”, *Earthquake Engineering and Structural Dynamics*, **44**, pp. 2057–2073 (2015). DOI:10.1002/eqe.2575.
44. Ruiz- García, J. and Aguilar, J.D. “Influence of modeling assumptions and aftershock hazard level in the seismic response of post-mainshock steel framed buildings”, *Engineering Structures*, **140**, pp. 437-446 (2017). DOI:10.1016/j.engstruct.2017.02.074
45. Zhang, Y. and Burton, H.V. “Pattern Recognition Approach to Assess the Residual Structural Capacity of Damaged Tall Buildings”, *Structural Safety*, **78**, pp. 12-22 (2019). DOI:10.1016/j.strusafe.2018.12.004
46. Amiri, S., Garakaninezhad, A. and Bojórquez, E. “Normalized residual displacement spectra for post-mainshock assessment of structures subjected to aftershocks”, *Earthquake Engineering and Engineering Vibration*, **20**(2), pp. 403-421 (2021). DOI:10.1007/s11803-021-2028-5
47. Lignos, D. “Sidesway Collapse of Deteriorating Structural Systems under Seismic Excitations”, Ph.D. Dissertation, Stanford University, California, USA (2008).
48. ASTM A6, “Standard Specification for General Requirements for Rolled Structural Steel Bars, Plates, Shapes, and Sheet Piling”, American Society for Testing and Materials, Pennsylvania, USA, (2016).
49. FEMA-350, “Recommended Seismic Design Criteria for New Steel Moment-Frame Buildings”, Federal Emergency Management Agency, Washington, DC, USA, (2000).
50. Mazzoni, S., McKenna, F., Scott, M.H., et al. “OpenSees Command Language Manual”, University of California, Berkeley, USA (2006). http://opensees.berkeley.edu/manuals/usermanual
51. Ibarra, L.F., Medina, R.A. and Krawinkler, H. “Hysteretic models that incorporate strength and stiffness deterioration”, *Earthquake Engineering and Structural Dynamics*, **34**(12), pp. 1489-1511 (2005). DOI:10.1002/eqe.495
52. Elkady, A. and Lignos, D.G. “Modeling of the composite action in fully restrained beam-to-column connections: implications in the seismic design and collapse capacity of steel special moment frames”, *Earthquake Engineering & Structural Dynamics*, **43**(13), pp. 1935-1954 (2014). DOI:10.1002/eqe.2430
53. Li, P. and Ellingwood, B.R. "Performance evaluation and damage assessment of steel frame buildings under main shock–aftershock earthquake sequences", *Earthquake Engineering and Structural Dynamics*, **36**, pp. 405–427 (2007). DOI:10.1002/eqe.667

Biographies

Mohsen Kalateh Ahani is an Assistant Professor of Structural Engineering at the University of Torbat Heydarieh (UTH) in Khorasan Razavi, Iran. He received his doctoral degree in Civil Engineering from Iran University of Science and Technology in 2014. Since joining the faculty at the UTH in 2015, Dr. Kalateh-Ahani has taught courses in mechanics of materials and structural analysis while conducting research in structural engineering. His primary research interests involve the optimal design of structures using metaheuristic algorithms, post-mainshock safety assessments of structures, and evaluating the residual collapse capacity of earthquake-damaged structures.

Homayoon E. Estekanchi is a Professor of Civil Engineering at Sharif University of Technology (SUT) in Tehran, Iran. He earned his doctoral degree in Civil Engineering from SUT in 1997 and has been a dedicated faculty member at the university since then, actively engaged in teaching and research for over 25 years. Dr. Estekanchi is a registered Professional Engineer and an esteemed member of several professional organizations, including the Iranian Construction Engineers Organization, the American Society of Civil Engineers, and the Iranian Inventors Association. His multidisciplinary research interests encompass a broad range of topics within the structural and earthquake engineering domains, with a particular emphasis on the design and analysis of tall buildings and industrial structures.

Appendix A

A list of table and figure captions are available in Table A.1 and Table A.2, respectively.

Table A.1. Table captions.

Table no.	Caption
1	Information of the earthquake sequences applied to the case-study building.

Table A.2. Figure captions.

Figure no.	Caption
1	A schematic illustration of the ET technique.
2	Visualization of the test steel office building: (a) 3D perspective, (b) floor view, (c) North-facing elevation, (d) A(2-4) moment-frame.
3	Damage histories of the test building under the three excitation records of the "ETA20kd" series and the corresponding RDSs.
4	Collapse capacity curves of the intact and mainshock-damaged test building under the aftershocks with positive and negative polarity.
5	Collapse capacity of the mainshock-damaged test building at the RDSs for the positive and negative polarities of the aftershocks.
6	The residual collapse capacity diagram of the test building under the earthquake sequences in Table 1 is depicted in (a) for the worst-case polarity and (b) for the mean kappa index and residual collapse capacity reductions.
7	Determination of the minimum kappa safety threshold for the test building.
8	Damage history of the test building under the 2015 Nepal mainshock-aftershock sequence: (a) the first scenario earthquake, (b) the second scenario earthquake.
9	Comparative collapse safety assessment of the test building for the two scenarios of the 2015 Nepal earthquake.

Appendix B

Tables and figures are provided in Table B.1 and Table B.2, respectively.

Table B.1. Tables of the manuscript.

Table

Table 1. Information of the earthquake sequences applied to the case-study building.

	Sequence ID	Mainshock	Aftershock	Polarity
1	kd0102+	ETA20kd01	ETA20kd02	+
2	kd0102−			−
3	kd0103+		ETA20kd03	+
4	kd0103−			−
5	kd0201+	ETA20kd02	ETA20kd01	+
6	kd0201−			−
7	kd0203+		ETA20kd03	+
8	kd0203−			−
9	kd0301+	ETA20kd03	ETA20kd01	+
10	kd0301−			−
11	kd0302+		ETA20kd02	+
12	kd0302−			−

Table B.2. Figures of the manuscript.

Figure
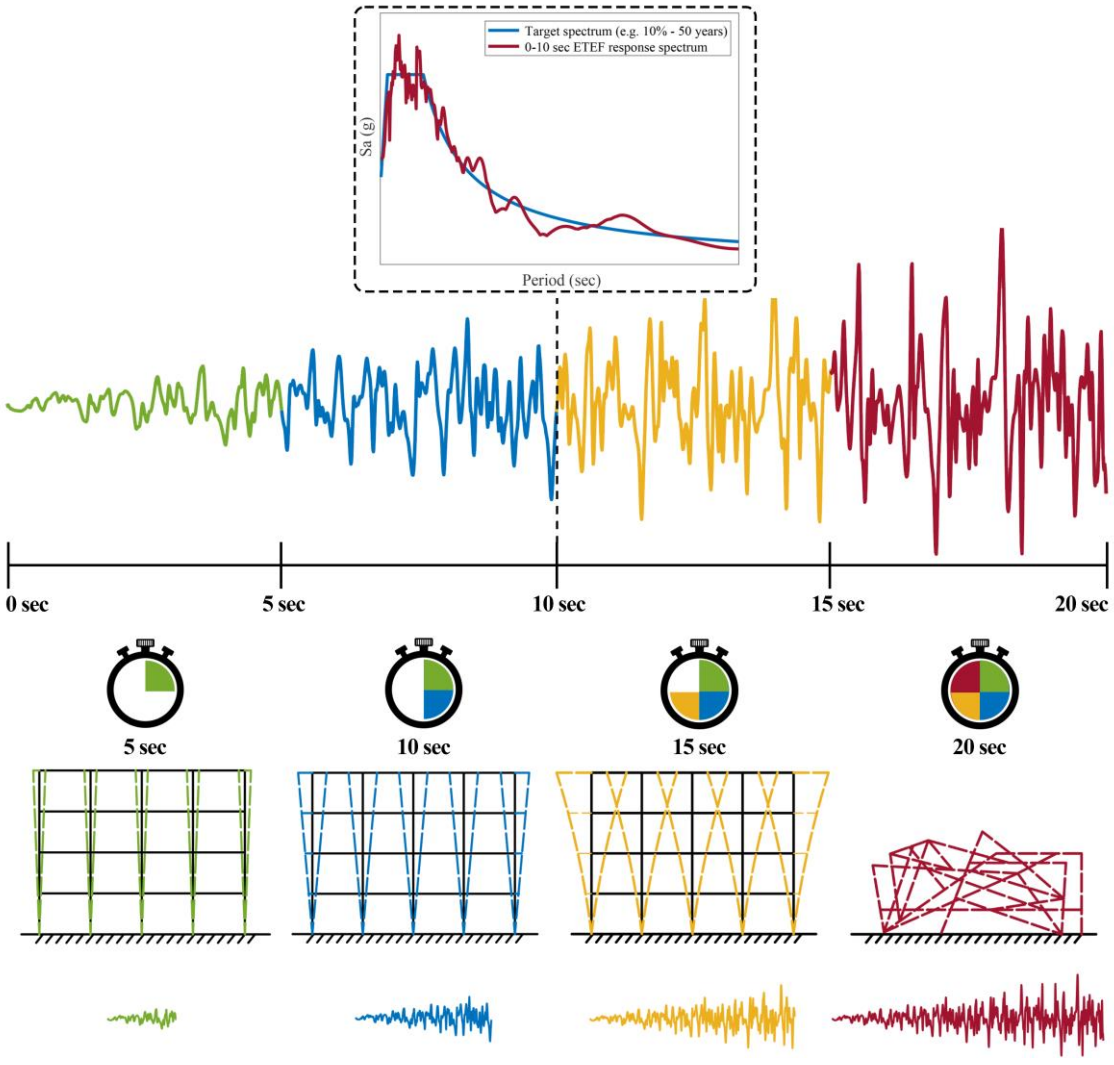

Figure 1. A schematic illustration of the ET technique.

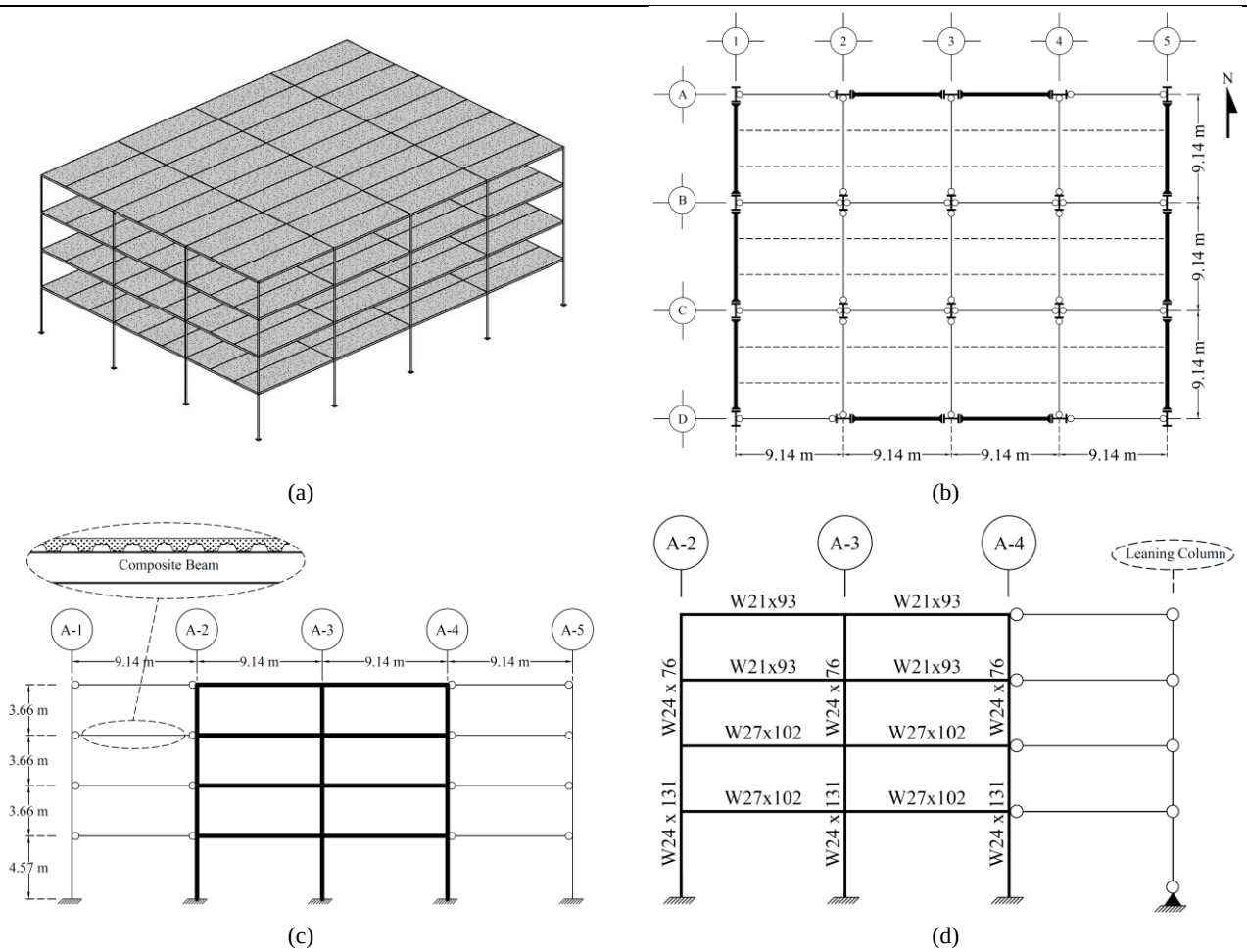

Figure 2. Visualization of the test steel office building: (a) 3D perspective, (b) floor view, (c) North-facing elevation, (d) A(2-4) moment-frame.

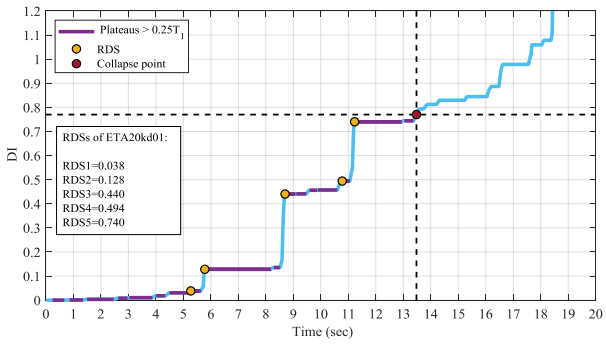

(a)

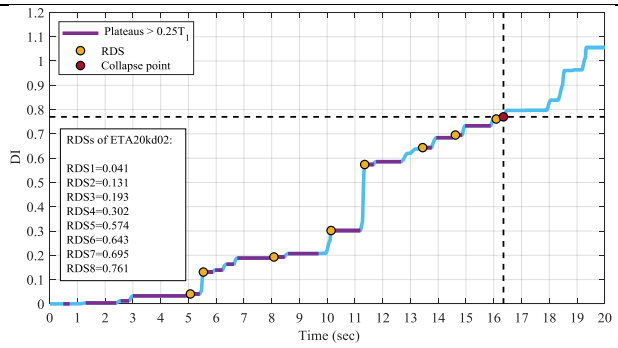

(b)

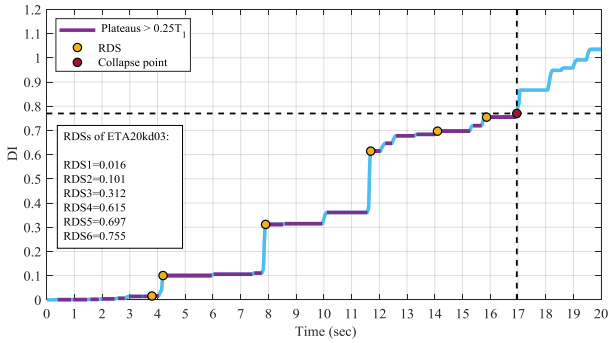

(c)

Figure 3. Damage histories of the test building under the three excitation records of the "ETA20kd" series and the corresponding RDSs.

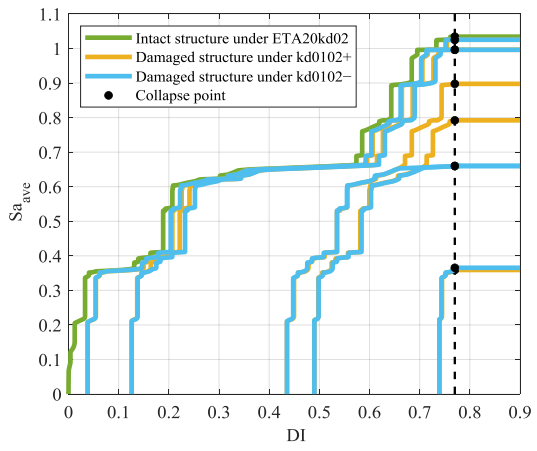

(a)

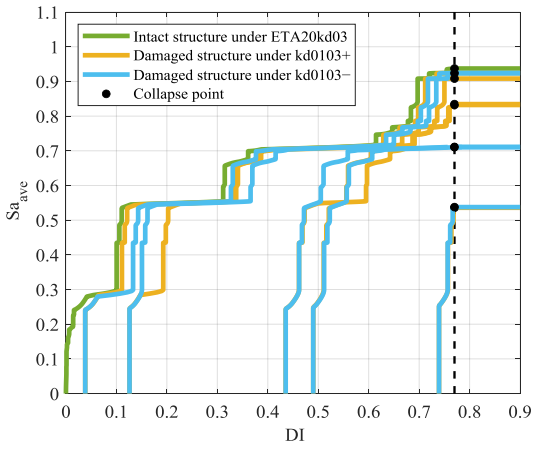

(b)

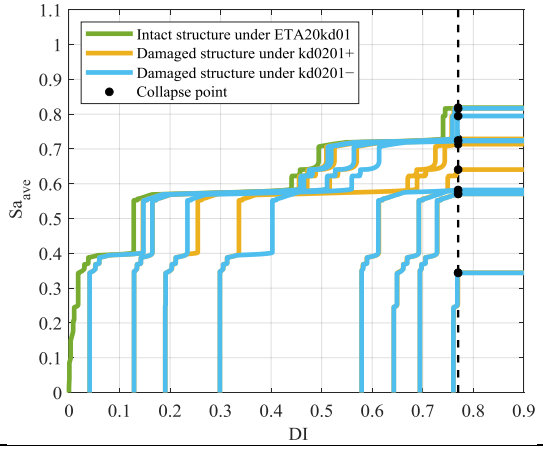

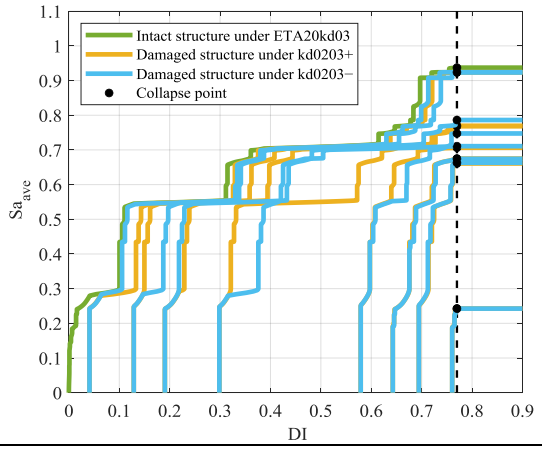

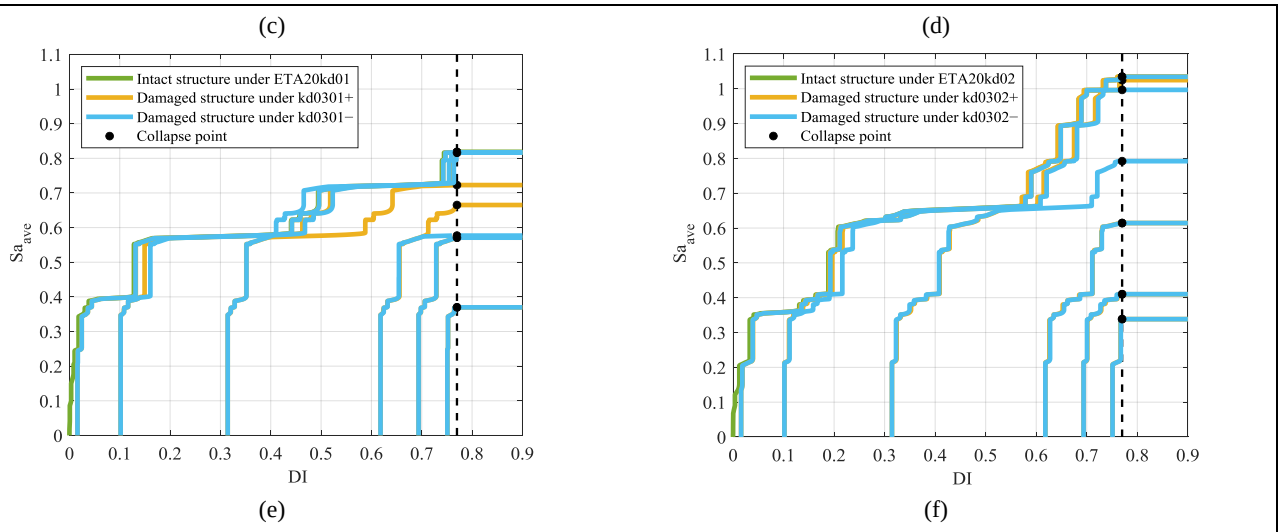

Figure 4. Collapse capacity curves of the intact and mainshock-damaged test building under the aftershocks with positive and negative polarity.

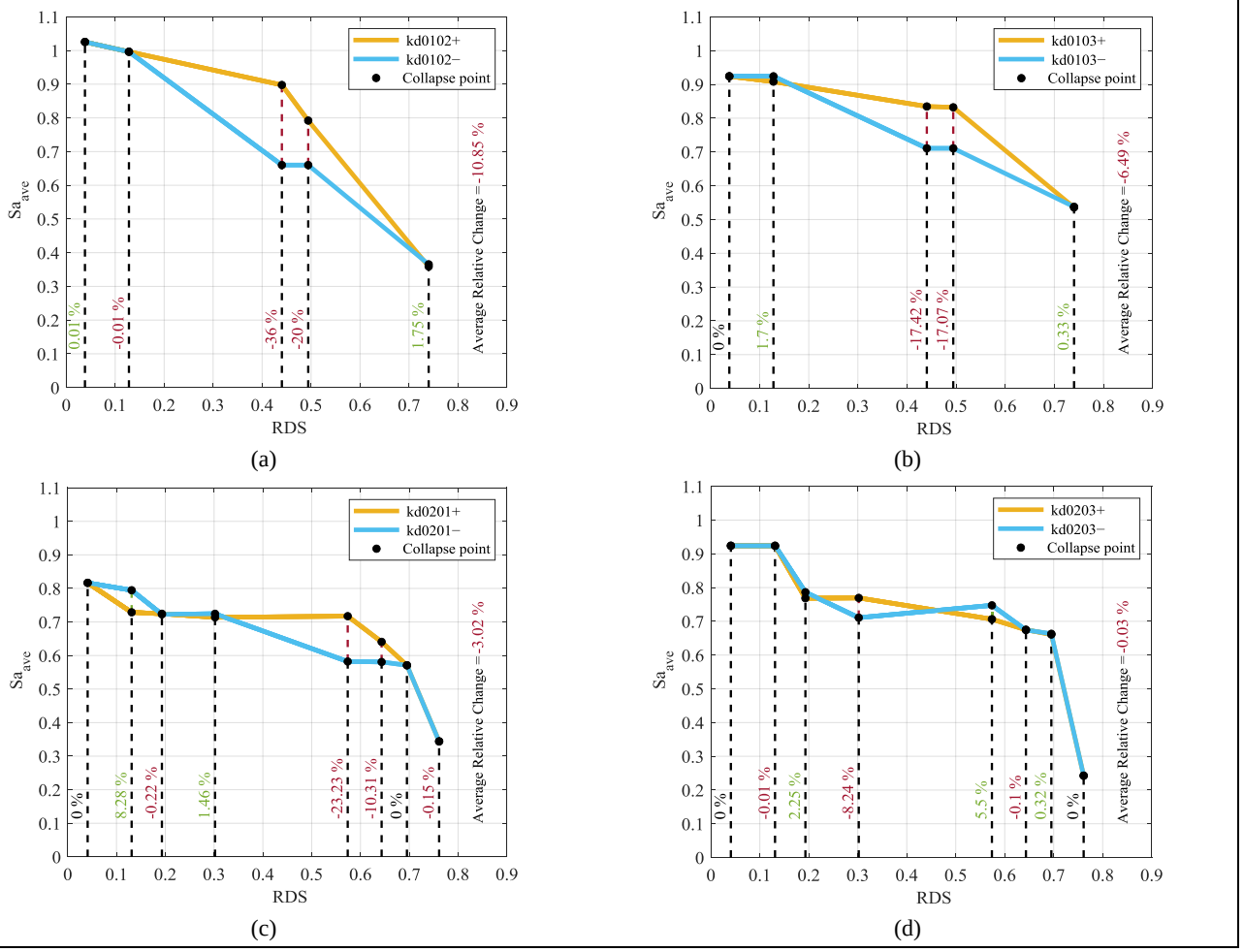

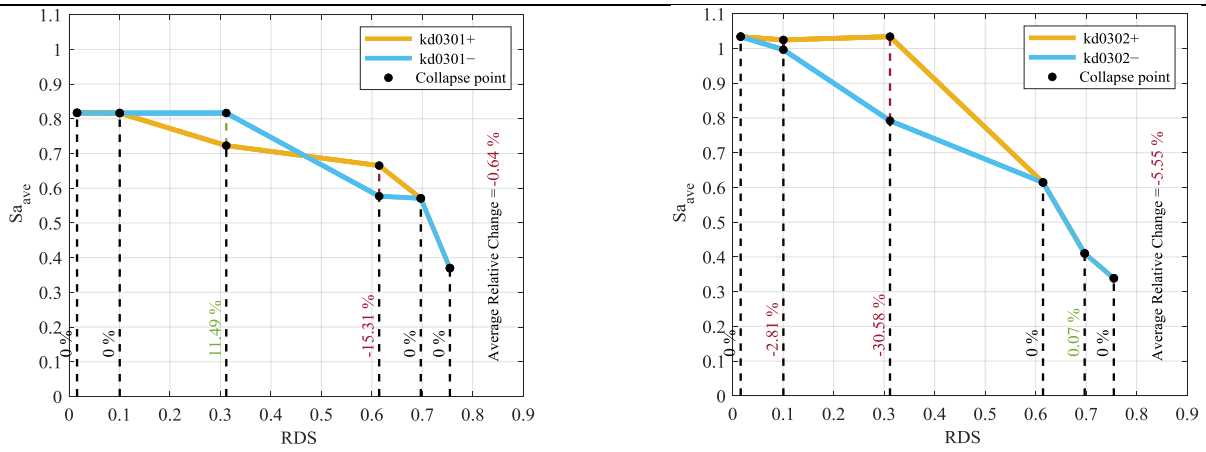

(e) (f)

Figure 5. Collapse capacity of the mainshock-damaged test building at the RDSs for the positive and negative polarities of the aftershocks.

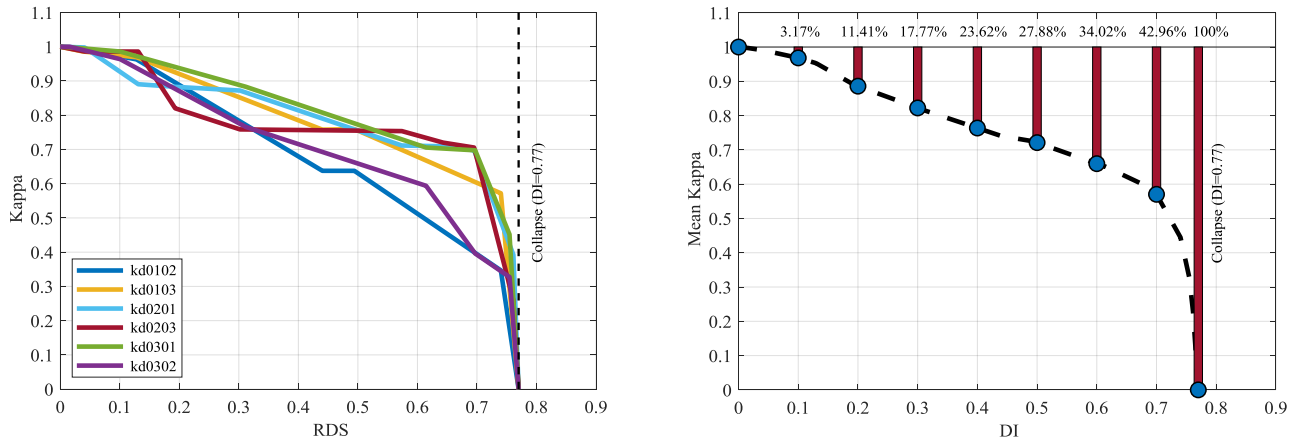

(a) (b)

Figure 6. The residual collapse capacity diagram of the test building under the earthquake sequences in Table 1 is depicted in (a) for the worst-case polarity and (b) for the mean kappa index and residual collapse capacity reductions.

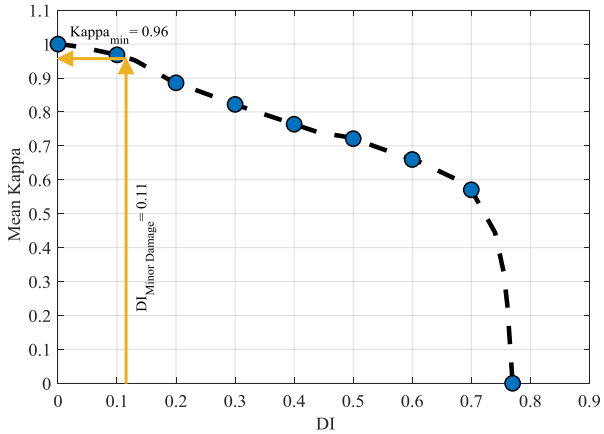

Figure 7. Determination of the minimum kappa safety threshold for the test building.

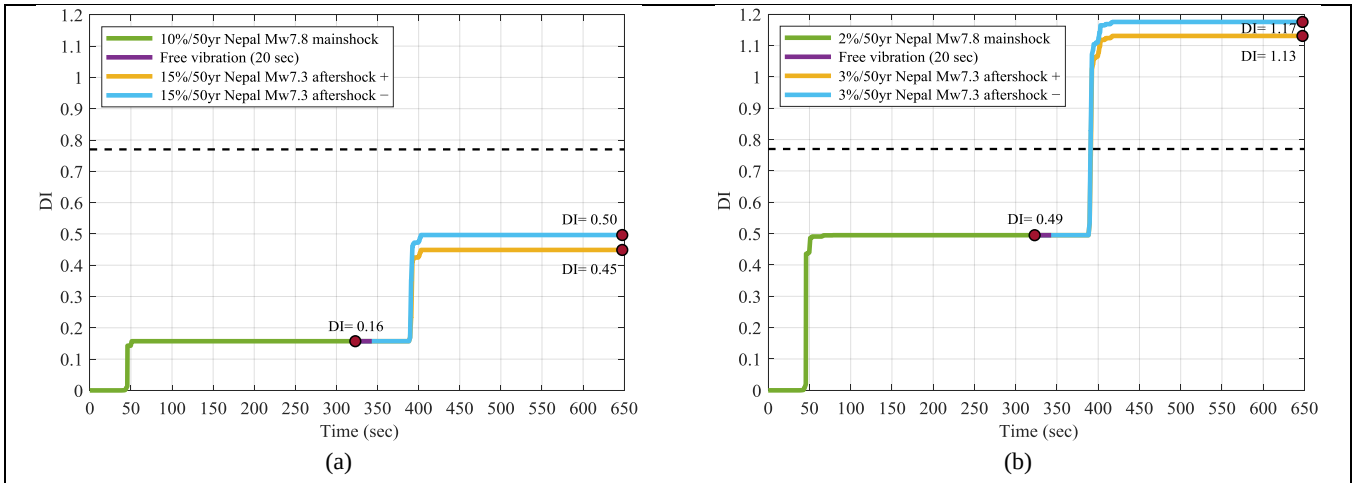

Figure 8. Damage history of the test building under the 2015 Nepal mainshock-aftershock sequence: (a) the first scenario earthquake, (b) the second scenario earthquake.

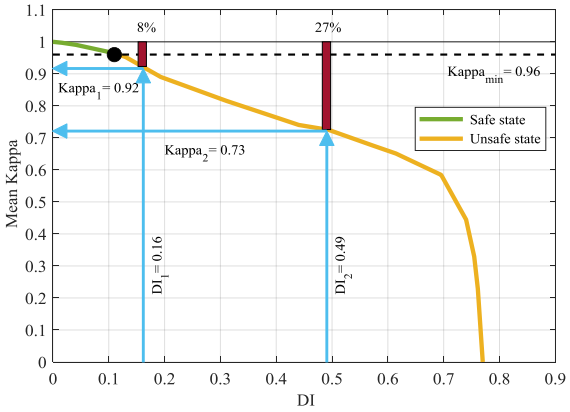

Figure 9. Comparative collapse safety assessment of the test building for the two scenarios of the 2015 Nepal earthquake.